

JCAS-MARL: Joint Communication and Sensing UAV Networks via Resource-Constrained Multi-Agent Reinforcement Learning

Islam Guven, Mehmet Parlak

ICTEAM, Université catholique de Louvain
Ottignies-Louvain-la-Neuve, Belgium
islam.guven@uclouvain.be

Abstract—Multi-UAV networks are increasingly deployed for large-scale inspection and monitoring missions, where operational performance depends on the coordination of sensing reliability, communication quality, and energy constraints. In particular, the rapid increase in overflowing waste bins and illegal dumping sites has created a need for efficient detection of waste hotspots. In this work, we introduce JCAS-MARL, a resource-aware multi-agent reinforcement learning (MARL) framework for joint communication and sensing (JCAS)-enabled UAV networks. Within this framework, multiple UAVs operate in a shared environment where each agent jointly controls its trajectory and the resource allocation of an OFDM waveform used simultaneously for sensing and communication. Battery consumption, charging behavior, and associated CO₂ emissions are incorporated into the system state to model realistic operational constraints. Information sharing occurs over a dynamic communication graph determined by UAV positions and wireless channel conditions. Waste hotspot detection requires consensus among multiple UAVs to improve reliability. Using this environment, we investigate how MARL policies exploit the sensing-communication-energy trade-off in JCAS-enabled UAV networks. Simulation results demonstrate that adaptive pilot-density control learned by the agents can outperform static configurations, particularly in scenarios where sensing accuracy and communication connectivity vary across the environment.

Index Terms—Multi-agent reinforcement learning (MARL), unmanned aerial vehicles (UAVs), joint communication and sensing (JCAS), OFDM radar, multi-UAV coordination, environmental monitoring, smart waste management, sustainability.

I. INTRODUCTION

Unmanned aerial vehicles (UAVs) equipped with 6G sub-terahertz (sub-THz) joint communication and sensing (JCAS) capabilities offer an approach for autonomous navigation, mission-critical data collection, and real-time environmental monitoring applications such as precision agriculture [1]. UAVs are increasingly used for environmental monitoring tasks including locating overflowing waste bins, detecting illegal dumping sites, and surveying hazardous hotspot regions [2]–[5]. Their high mobility, flexible deployment, and low operational cost make them well suited for rapid inspection of large areas. However, limited onboard battery capacity, intermittent connectivity, and variability in sensing performance constrain the effectiveness of UAV operations. These chal-

lenges make coordinated multi-UAV exploration and information sharing a dynamic multi-objective optimization problem, where sensing performance, communication reliability, and energy efficiency must be jointly considered.

These operational trade-offs are fundamentally influenced by the underlying communication and sensing mechanisms. Recent developments in JCAS systems provide a physical-layer framework for capturing the interaction between sensing performance and communication capability. Communication-centric JCAS architectures reuse a single OFDM waveform for both radar-style sensing and data communication [6], [7]. Pilot symbols allow echo estimation and improve sensing signal-to-noise ratio (SNR), while data symbols determine throughput. Adjusting the pilot density therefore controls the balance between communication and sensing. Increasing pilot allocation strengthens sensing but reduces communication capacity. Studies on energy-efficient UAV communication further show that such physical-layer choices interact with sustainability constraints [8]. The literature on environmental UAVs also emphasizes the operational importance of reliable sensing for waste management [9], [10].

Multi-agent reinforcement learning (MARL) provides an approach for coordinating UAV teams under these coupled physical constraints [11], [12]. However, existing MARL environments typically abstract away JCAS effects, assume deterministic sensing, or ignore time-varying communication graphs. Furthermore, these models do not allow control over waveform-level decisions. To address this gap, we propose a sustainability-aware MARL framework in which each UAV controls its motion and its OFDM pilot density. This joint action space enables the policy to modulate sensing and communication quality as operational conditions evolve. Battery usage, renewable-aware charging, and CO₂ emissions are integrated into the environment in order to allow carbon-aware decision making during multi-UAV waste hotspot detection. The contributions of this paper are as follows:

- We develop a partially-observable MARL environment that optimizes grid-based UAV mobility with an OFDM-based sensing and communication layer, including energy usage, CO₂ emissions, and knowledge propagation.

- We propose a joint action representation in which each agent controls both its motion and pilot density, allowing adaptive management of sensing quality and communication connectivity under partial observability.
- We experimentally demonstrate how PPO policies exploit the waveform capacity across varying fleet sizes and hotspot densities, showing gains in success rate, mission time, and communication efficiency over a constant pilot-density baseline.

The remainder of this paper is structured as follows. Section II presents the system model, including the grid layout, the OFDM-based joint sensing-and-communication formulation, and the energy and sustainability framework. Section III describes the MARL formulation, action and observation spaces, reward design, and the multi-hop knowledge propagation mechanism. Section IV reports the experimental results, including sensing–communication trade-offs and sustainability outcomes. Section V concludes the paper and discusses possible extensions.

II. SYSTEM MODEL

We consider a 2D grid $G = (V, E)$ with square cell size d meters, where V denotes the set of grid cells and E represents the edges between neighboring cells. The grid contains $|V| = W \times H$ cells, with W and H denoting its width and height. A set of N UAVs, $\mathcal{U} = \{1, \dots, N\}$ navigates by moving to one of the 4-neighbors of its current cell or staying. Depots $\mathcal{D} \subset V$ provide charging with electricity under a carbon intensity c_t (kgCO₂/kWh) [13].

Each mission starts with a random placement of waste hotspots, \mathcal{T}^w . A hotspot is detected when multiple UAVs achieve sufficiently strong JCAS sensing SNR. A schematic overview of the sensing task is shown in Fig. 1.

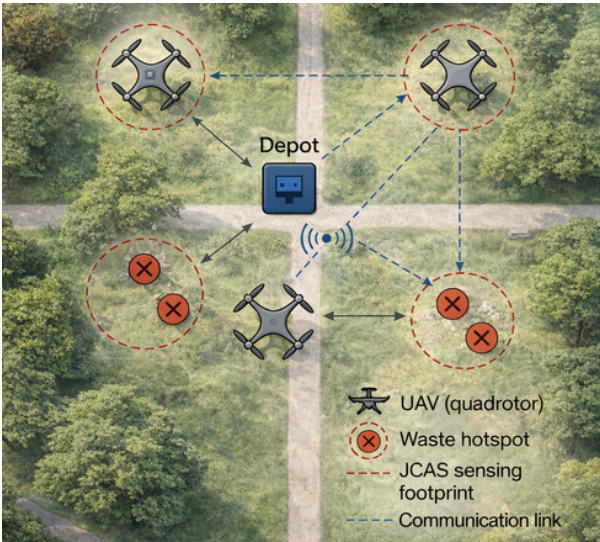


Fig. 1: Illustration of the UAV waste-hotspot localization mission, in which a team of UAVs is deployed from a central depot that acts as a base station and patrols the designated grid area.

A. JCAS Sensing and Communication Model

Each UAV transmits a single OFDM waveform that is used both for sensing of waste hotspots and for maintaining a communication link. The OFDM configuration is fixed throughout the mission, the only JCAS-related degree of freedom exposed to the policy is the pilot density $\rho_i^{\text{pilot}}(t)$, which controls how much of the time–frequency grid is reserved for pilots instead of data transmission. The remaining fraction

$$\rho_i^{\text{comm}}(t) = 1 - \rho_i^{\text{pilot}}(t)$$

is the communication load. This scalar control ties together sensing reliability and communication quality.

Table I summarizes the main physical-layer parameters used by the JCAS model and the scale at which they operate. These values are kept constant during training; all adaptation comes from the learned pilot-density decisions and the resulting UAV trajectories.

We adopt a monostatic OFDM radar model. UAV i uses a waveform centered at carrier frequency f_c with bandwidth B . The received echo power from hotspot j is

$$P_{r,ij}(t) = \frac{P_t G_t G_r \lambda^2 \sigma_j}{(4\pi)^3 R_{ij}(t)^4}, \quad (1)$$

where $\lambda = c/f_c$ and $R_{ij}(t)$ is the UAV–hotspot distance computed from the grid using cell size d .

The sensing SNR in dB is then

$$\text{SNR}_{ij}^{\text{sens}}(t) = 10 \log_{10} \left(\frac{P_{r,ij}(t)}{P_n} \right) + G_{\text{proc}} - \Delta_{\text{res}}(R_{ij}(t)), \quad (2)$$

where $\Delta_{\text{res}}(\cdot)$ is a fixed range-resolution penalty.

Communication load reduces sensing quality by lowering pilot allocation. The effective sensing SNR is

$$\widetilde{\text{SNR}}_{ij}^{\text{sens}}(t) = \text{SNR}_{ij}^{\text{sens}}(t) - \alpha_{\text{JCAS}} \rho_i^{\text{comm}}(t). \quad (3)$$

The detection margin is defined as

$$m_{ij}(t) = \widetilde{\text{SNR}}_{ij}^{\text{sens}}(t) - \gamma_{\text{det}}, \quad (4)$$

and mapped to a detection probability via

$$p_{ij}(t) = \frac{1}{1 + \exp(-\kappa m_{ij}(t))}. \quad (5)$$

TABLE I: JCAS parameters.

Symbol	Value	Role
f_c	5.8 GHz	Carrier frequency of OFDM waveform.
B	100 MHz	Total bandwidth; sets radar resolution scale.
P_t	20 dBm	Transmit power per UAV.
G_t, G_r	2 dBi	TX/RX antenna gains.
σ_j	0 dBsm	Effective radar cross section of hotspot j .
P_n	−90 dBm	Sensing noise floor.
G_{proc}	8 dB	OFDM processing gain (coherent combining).
d	50 m	Physical size of one grid cell.
n	2.0	Path-loss exponent for communication SNR.
ρ_i^{pilot}	[0.01, 0.30]	Pilot density chosen by UAV i .
α_{JCAS}	1.0 dB	Sensing SNR penalty per unit comm load.
γ_{det}	derived	Effective detection threshold (dB).
κ	0.25	Slope of logistic detection curve.

A hotspot j is considered detected at time t if at least θ_{detect} UAVs provide a positive detection:

$$\sum_{i=1}^N \mathbb{1}[\text{detect}_{ij}(t)] \geq \theta_{\text{detect}}. \quad (6)$$

Communication uses the same OFDM waveform, with a log-distance path-loss model and noise floor returning pairwise SNR $_{i,j}^{\text{comm}}(t)$ between each UAV i and j . The communication load $\rho_i^{\text{comm}}(t)$ determines how much of the resource grid supports data transfer. These SNR-derived connectivity metrics define the communication graph through which detections propagate.

Overall, the MARL policy learns to jointly adjust $\rho_i^{\text{pilot}}(t)$ and UAV trajectories so that sensing confidence, communication reliability, and multi-UAV knowledge propagation are balanced across multiple hotspots. More details on partial observability and knowledge propagation are given in Sec. III-D.

B. Energy and Carbon Model

Each agent i holds battery capacity $b_i(t) \in [0, B_{\text{max}}]$. Per step,

$$e_i(t) = e_{\text{move}}(a_i(t)) + e_{\text{sense}}(i, t) + e_{\text{comm}}(i, t), \quad (7)$$

$$b_i(t+1) = \min\{B_{\text{max}}, b_i(t) - e_i(t) + \chi_i(t) r_{\text{ch}}\}, \quad (8)$$

where e_{move} is the propulsion cost (assumed to be constant per move), e_{sense} depends on pilot density and sensing activity, e_{comm} accounts for communication overhead, $\chi_i(t) = 1$ if at a depot, and r_{ch} is the charging rate (kWh/step). Charging energy splits into renewable energy share ρ_{RE} and grid energy:

$$e_i^{\text{grid}}(t) = (1 - \rho_{\text{RE}}) \chi_i(t) r_{\text{ch}}, \quad \text{CO}_2(t) = \sum_i e_i^{\text{grid}}(t) c_t. \quad (9)$$

C. Task Completion

A hotspot j is detected at t_j^{det} when the JCAS multi-sensor condition above is met and informed when all agents have the hotspot in their binary knowledge vectors (Sec. III-D). When all hotspots are informed, the mission is completed.

III. MARL FORMULATION

We define a Dec-POMDP $\langle \mathcal{N}, \mathcal{S}, \{\mathcal{A}_i\}, P, R, \{\Omega_i\}, O, \gamma \rangle$ [11], [12]. Each agent controls both motion and JCAS waveform configuration.

A. Action Space

Each agent i selects a continuous 2D action:

$$\mathbf{a}_i(t) = (u_i^{\text{dir}}(t), u_i^{\text{pilot}}(t)) \in [-1, 1]^2. \quad (10)$$

The first component u_i^{dir} is mapped to one of five motions {up, down, left, right, stay}. The second component u_i^{pilot} is mapped to a pilot density

$$\rho_i^{\text{pilot}}(t) = \rho_{\text{min}} + \frac{u_i^{\text{pilot}}(t) + 1}{2} (\rho_{\text{max}} - \rho_{\text{min}}), \quad (11)$$

clipped to $[\rho_{\text{min}}, \rho_{\text{max}}]$, with $\rho_i^{\text{comm}}(t) = 1 - \rho_i^{\text{pilot}}(t)$. Therefore, the MARL policy must co-design UAV trajectories and JCAS resource allocation.

B. Reward Design with JCAS and Sustainability Signals

We combine sparse task outcomes with dense JCAS and sustainability shaping:

$$\begin{aligned} R_t = & \underbrace{\sum_{j \in \mathcal{T}^w} (\alpha_{\text{det}} \mathbb{1}[t=t_j^{\text{det}}] + \alpha_{\text{inf}} \mathbb{1}[\text{informed}_j(t)])}_{\text{waste detection \& informing}} \\ & + \underbrace{\alpha_{\text{comp}} \mathbb{1}[\text{all hotspots informed at } t]}_{\text{completion reward}} \\ & + \underbrace{\alpha_{\text{cov}} \cdot \text{coverage_gain}(t)}_{\text{coverage reward}} \\ & - \underbrace{\eta_e \sum_i e_i(t)}_{\text{energy penalty}} - \underbrace{\eta_c \sum_i e_i^{\text{grid}}(t) c_t}_{\text{carbon penalty}} \\ & - \underbrace{\xi_{\text{rev}} \cdot \text{revisit_count}(t) + \xi_{\text{trunc}} \mathbb{1}[t=T_{\text{max}}]}_{\text{efficiency penalties}} \\ & + \underbrace{\zeta_{\text{comm}} \cdot \bar{\eta}(t)}_{\text{communication throughput reward}} \\ & + \underbrace{\zeta_{\text{spread}} \cdot \text{knowledge_spread}(t)}_{\text{propagation bonus}}. \end{aligned} \quad (12)$$

where $\bar{\eta}(t)$ is the average normalized communication throughput across agents at time t , and $\text{knowledge_spread}(t)$ measures the fraction of agents that know each detected hotspot. We use potential-based terms for distance-to-goal (nearest undetected hotspot) and for carbon-aware charging (encouraging charging at depots with high ρ_{RE} or low c_t) to preserve optimality [14].

C. Observations

Each agent receives a local observation $\mathbf{o}_i(t)$ including:

- **Self:** normalized position on the grid, battery SoC $b_i(t)/B_{\text{max}}$, current pilot density $\rho_i^{\text{pilot}}(t)$, and a coarse estimate of its own communication SNR or throughput.
- **Targets:** for each waste hotspot j : relative grid position, detection status, and agent knowledge bit $k_{ij}(t)$.
- **Other UAVs/Comm:** relative positions of neighbors within communication radius, and an aggregated measure of JCAS connectivity.
- **Sustainability:** current carbon intensity c_t and distance to nearest depot.
- **Global progress:** fractions of detected/informed hotspots, and normalized time index.

D. Knowledge Propagation

After JCAS sensing, each agent updates its binary knowledge vector $\mathbf{k}_i(t)$ based on local detections, then runs a multi-iteration consensus step over the communication graph. $\mathcal{N}_i(t)$ is the communication neighbors of agent i at time t and $\mathbf{k}_i^{(0)}(t)$ the post-sensing vector. For $\ell = 1, \dots, N$,

$$\mathbf{k}_i^{(\ell)}(t) \leftarrow \mathbf{k}_i^{(\ell-1)}(t) \bigvee_{j \in \mathcal{N}_i(t)} \mathbf{k}_j^{(\ell-1)}(t), \quad (13)$$

where \vee denotes the elementwise logical OR. Therefore, each connected component of the communication graph becomes aware of the detected hotspots in a single environment step [15].

E. Training Algorithm

We use centralized training with decentralized execution (CTDE) [16]. Policies are shared across agents and trained with Synchronous PPO with GAE [17], [18], collecting batches synchronously from all actors. Policies use 3-layer MLP architectures (512-256-128 units). We implement the MARL training pipeline using Ray RLlib [19].

IV. RESULTS

A. Environment setup

We consider a 12×12 grid with cell size $d = 50\text{m}$ and a mission horizon of $T_{\max} = 100$, which corresponds to the operational endurance implied by a 0.20kWh battery per UAV. We evaluate fleets of $N \in \{5, 10, 15, 20\}$ UAVs and hotspot configurations with $n_{\text{targets}} \in \{3, 5, 7, 9, 11\}$ waste locations generated randomly for each episode.

TABLE II: Experiment Configuration for Sustainability-Aware JCAS-MARL Training and Evaluation

Category	Parameter	Value
Environment Configuration		
Grid size	$W \times H$	12×12 cells
Cell size	d	50 m
Number of UAVs	N	$\{5, 10, 15, 20\}$
Number of hotspots	n_{targets}	$\{3, 5, 7, 9, 11\}$
Max steps per episode	T_{\max}	100
Detection threshold	θ_{detect}	3 UAVs
Energy and Sustainability Model		
Battery capacity	B_{\max}	0.20 kWh
Return-to-base threshold		0.04 kWh
Charge rate	r_{ch}	0.30 kW
Movement cost	e_{move}	8×10^{-4} kWh
Sensing energy	e_{sense}	2×10^{-4} kWh
Communication energy	e_{comm}	5×10^{-5} kWh
Renewable energy share	ρ_{RE}	0.1
Grid CO ₂ intensity	c_t	$[0.25 - 0.40]$ kg/kWh
Reward Weights		
Correct detection reward		7.0
Inform reward		4.0
Completion reward		10.0
Coverage reward		0.5
Revisit penalty		-0.01
Truncation penalty		-0.4
Energy penalty coefficient		0.2
Carbon penalty coefficient		0.1
Communication throughput reward		0.5
Knowledge spread reward		0.1
MARL / PPO Configuration		
Algorithm		PPO (CTDE)
Discount factor	γ	0.95
Learning rate	α	3×10^{-4}
Batch size		4096
Training steps		2.5×10^5
Episodes per evaluation	M	100

The carbon intensity of the charging station (depot) c_t is sampled uniformly in the range $[0.25, 0.40]$ kg/kWh at each step, mimicking a time-varying grid mix.

The joint communication-and-sensing layer uses a single OFDM waveform at 5.8GHz with 100MHz bandwidth with parameters defined in Sec. II. Each UAV controls only its pilot density, which is bounded within $[0.01, 0.30]$ and determines the sensing-communication resource split. A hotspot is confirmed when at least $\theta_{\text{detect}} = 3$ UAVs detect it in the same step, and a mission is successful only if all hotspots are detected and informed to all UAVs. Additional parameters are included in Table II.

B. Training Costs

Table III summarizes the PPO training costs for different fleet sizes on our Intel Xeon Gold 6444Y CPU with 8 parallel processes. Each evaluation rollout takes on the order of 1–2 s.

TABLE III: PPO training times in seconds for different fleet sizes.

Method	$N=5$	$N=10$	$N=15$	$N=20$
PPO	402	598	1253	1751

C. PPO Convergence Across Target Densities

Fig. 2 shows the evolution of the mean episode return as a function of PPO training iterations for different numbers of hotspots. One PPO iteration corresponds to sampling one full batch of 4096 environment steps and performing 10 epochs of gradient updates. Across all target sets, the return stabilizes after around 40 iterations, indicating that PPO can reliably learn a joint trajectory and pilot-density policy in this JCAS-enabled environment.

D. Effect of Fleet Size on Detection Performance

We next evaluate the learned PPO policies in terms of mission success. Fig. 3 reports the evaluation success rate as a function of the number of UAVs for 3 – 11 targets on the same region. The curves show that fleets of 10 UAVs already

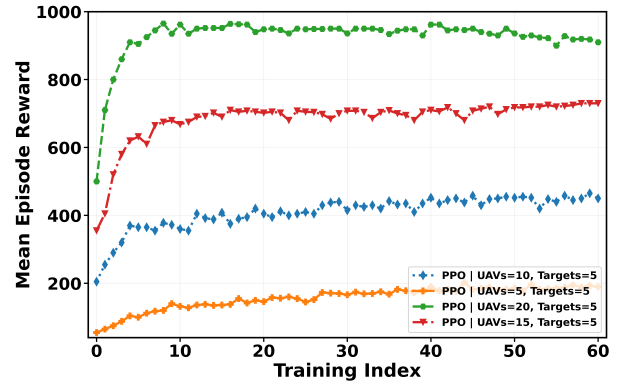


Fig. 2: Training evolution of the mean episode return for different numbers of targets.

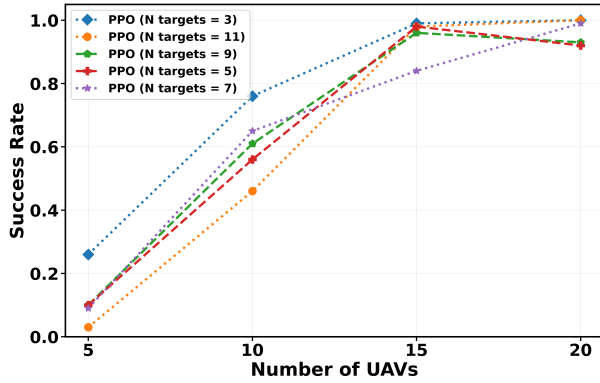


Fig. 3: Evaluation success rate as a function of the number of UAVs for 3 – 11 targets.

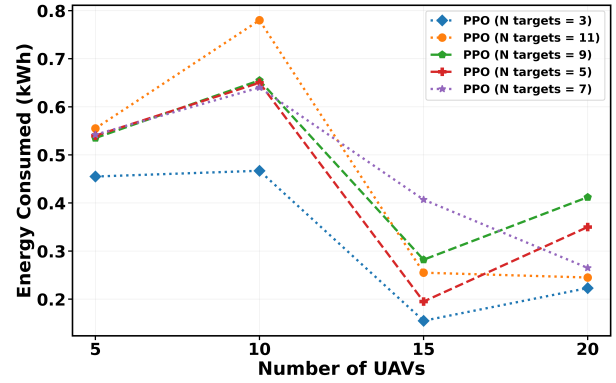


Fig. 5: Total energy consumption per mission as a function of the number of UAVs.

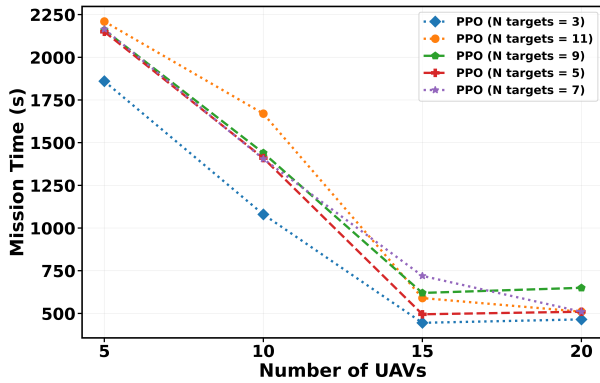


Fig. 4: Evaluation mission time as a function of the number of UAVs.

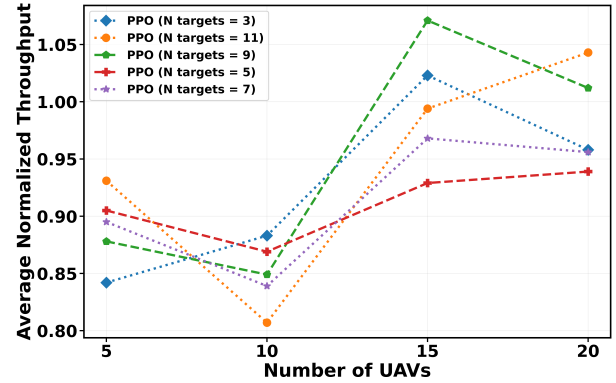


Fig. 6: Normalized communication throughput as a function of the number of UAVs.

achieve an average success rate around 0.73, while 15 UAVs reach approximately 97% success for all three target densities.

Fig. 4 shows the corresponding mission times. As the fleet size grows, mission time decreases sharply and then saturates once the team is large enough to cover the region and confirm all hotspots without long waiting times.

E. Energy Consumption and Communication Throughput

To quantify sustainability, Fig. 5 reports the total energy consumption per mission versus the number of UAVs. Although larger fleets consume more energy in aggregate, the increase is sublinear in N because better coverage reduces redundant motion and repeated hotspot visits.

Finally, Fig. 6 illustrates the normalized communication throughput obtained from the OFDM-based JCAS model as a function of fleet size. The learned policies keep pilot density high when approaching suspected hotspots and reduce it afterwards, preserving enough throughput to propagate detections through the communication graph even for larger teams. Because throughput is normalized using a fixed reference spectral efficiency of 6 bits/s/Hz, episodes with high communication SNR can return normalized throughput values above 1.

F. Constant Pilot Density Model

We also analyze the success rate of a constant pilot density model where pilot density is set at 0.3 for allowing both communication and sensing without adaptivity. Fig. 7 shows that with larger fleets, the improvement of success rates reach around 10% while for 10 UAVs, both models have fluctuating advantages around 5%. This shows that adaptivity is not

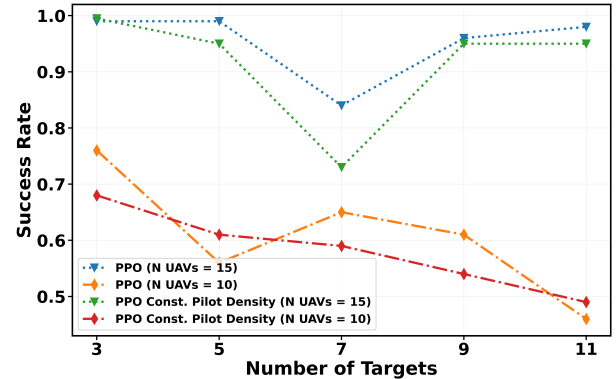


Fig. 7: Evaluation success rate as a function of the number of Hotspots.

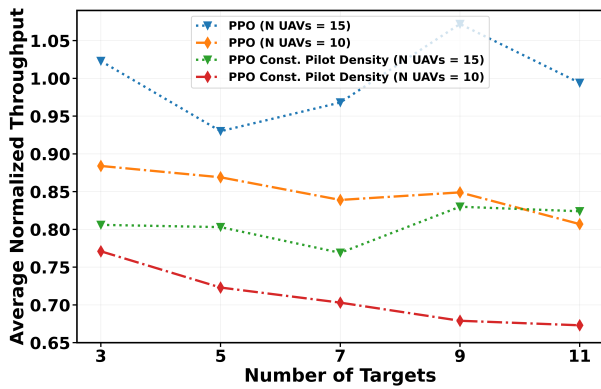


Fig. 8: Normalized communication throughput as a function of the number of Hotspots.

always an advantage, and larger target numbers reduce the need for adaptivity since the mission gets closer to an area coverage mission.

To further analyze the effect of throughput on pilot density, we compare the average throughput for 10 and 15 UAVs for both configurations in Fig. 8. With a constant pilot rate, UAVs can no longer take advantage of boosting communication power on situations where there is no need for sensing which results in a reduced average throughput.

V. CONCLUSION

We demonstrated a sustainability- and JCAS-aware MARL framework for UAV-based waste hotspot response that integrates battery dynamics, energy consumption, carbon emissions, and joint communication-and-sensing signals into the learning process. A monostatic OFDM radar-communication model replaces range-based abstractions, allowing agents to adapt pilot density to balance sensing reliability and communication throughput.

Simulation results in a 12×12 grid environment with fleets of 5–20 UAVs and 3–11 hotspots show that PPO agents learn stable policies within about 40 training iterations, with training times ranging from 402 s to 1751 s depending on fleet size. The learned policies achieve high mission success rates, reaching approximately 0.73 with 10 UAVs and about 97% with 15 UAVs across target densities, while reducing mission time as fleet size increases. Despite larger teams consuming more total energy, the growth is sublinear due to improved spatial coverage. Furthermore, adaptive pilot-density control maintains reliable communication throughput while enabling multi-sensor confirmation of hotspots, outperforming fixed pilot configurations in several scenarios.

These results demonstrate that integrating sustainability-aware objectives and JCAS resource control within MARL enables coordinated UAV policies that effectively detect waste hotspots while balancing sensing reliability, communication performance, and energy use.

ACKNOWLEDGMENT

This work was supported by the Brains for Brussels research and innovation funding program of the Région de Bruxelles-Capitale-Innoviris under Grant RBC/BFB 2023-BFB-2.

REFERENCES

- [1] I. Guven and M. Parlak, “Blockchain, AI and IoT Empowered Swarm Drones for Precision Agriculture Applications,” in *2022 IEEE 1st Global Emerging Technology Blockchain Forum: Blockchain and Beyond (iGETBlockchain)*, 2022, pp. 1–6.
- [2] S. Waharte and N. Trigoni, “Supporting Search and Rescue Operations with UAVs,” *2010 International Conference on Emerging Security Technologies*, pp. 142–147, 2010.
- [3] M. A. Goodrich, B. S. Morse, D. Gerhardt, J. L. Cooper, M. Quigley, J. A. Adams, and C. Humphrey, “Supporting wilderness search and rescue using a camera-equipped mini UAV,” *Journal of Field Robotics*, vol. 25, no. 1-2, pp. 89–110, 2008.
- [4] M. Erdelj, M. Król, and E. Natalizio, “Help from the Sky: Leveraging UAVs for Disaster Management,” *IEEE Pervasive Computing*, vol. 16, no. 1, pp. 24–32, 2017.
- [5] C. Vincent-Lambert, A. Pretorius, and B. Van Tonder, “Use of Unmanned Aerial Vehicles in Wilderness Search and Rescue Operations: A Scoping Review,” *Wilderness and Environmental Medicine*, vol. 34, no. 4, pp. 580–588, 2023.
- [6] L. Zhou, S. Leng, Q. Wang, and Q. Liu, “Integrated Sensing and Communication in UAV Swarms for Cooperative Multiple Targets Tracking,” *IEEE Transactions on Mobile Computing*, vol. 22, no. 11, pp. 6526–6542, 2023.
- [7] X. Chen, Z. Feng, Z. Wei, F. Gao, and X. Yuan, “Performance of joint sensing-communication cooperative sensing UAV network,” *IEEE Transactions on Vehicular Technology*, vol. 69, no. 12, pp. 15 545–15 556, 2020.
- [8] A. Ranjha, D. Naboulsi, M. E. Emary, and F. Gagnon, “Consumer-Centric Sustainability: Empowering URLLC in Multi-UAV-Assisted MEC Systems for Industry 5.0,” *IEEE Transactions on Consumer Electronics*, vol. 71, no. 2, pp. 4304–4316, 2025.
- [9] A. Younesi, H. S. Fard, A. B. Yengikand, and V. Pezeshki, “Survey on IoT-based Waste Management Systems,” in *2022 8th International Conference on Web Research (ICWR)*, 2022, pp. 162–167.
- [10] J. C. Hodgson, R. Mott, S. M. Baylis, T. T. Pham, S. Wotherspoon, A. D. Kilpatrick, R. R. Segaran, I. Reid, A. Terauds, and L. P. Koh, “Drones count wildlife more accurately and precisely than humans,” *Methods in Ecology and Evolution*, vol. 9, no. 5, pp. 1160–1167, 2018.
- [11] K. Zhang, Z. Yang, and T. Başar, “Multi-Agent Reinforcement Learning: A Selective Overview of Theories and Algorithms,” *Handbook of Reinforcement Learning and Control*, pp. 321–384, 2021.
- [12] R. Lowe, Y. I. Wu, A. Tamar, J. Harb, O. Pieter Abbeel, and I. Mordatch, “Multi-Agent Actor-Critic for Mixed Cooperative-Competitive Environments,” in *Advances in Neural Information Processing Systems*, 2017, pp. 6379–6390.
- [13] S. Forti, J. Soldani, and A. Brogi, “Carbon-aware Software Services,” 2024. [Online]. Available: <https://arxiv.org/abs/2405.12582>
- [14] A. Y. Ng, D. Harada, and S. Russell, “Policy invariance under reward transformations: Theory and application to reward shaping,” in *International Conference on Machine Learning*, vol. 99, 1999, pp. 278–287.
- [15] R. Olfati-Saber, J. A. Fax, and R. M. Murray, “Consensus and Cooperation in Networked Multi-Agent Systems,” *Proceedings of the IEEE*, vol. 95, no. 1, pp. 215–233, 2007.
- [16] L. Kraemer and B. Banerjee, “Multi-agent reinforcement learning as a rehearsal for decentralized planning,” *Neurocomputing*, vol. 190, pp. 82–94, 2016.
- [17] J. Schulman, F. Wolski, P. Dhariwal, A. Radford, and O. Klimov, “Proximal policy optimization algorithms,” *arXiv preprint arXiv:1707.06347*, 2017.
- [18] J. Schulman, P. Moritz, S. Levine, M. Jordan, and P. Abbeel, “High-Dimensional Continuous Control Using Generalized Advantage Estimation,” *arXiv preprint arXiv:1506.02438*, 2015.
- [19] E. Liang, R. Liaw, R. Nishihara, P. Moritz, R. Fox, K. Goldberg, J. Gonzalez, M. Jordan, and I. Stoica, “RLlib: Abstractions for distributed reinforcement learning,” in *International Conference on Machine Learning*, 2018, pp. 3053–3062.